Microfluidic platform for selective microparticle parking and paired particle isolation in droplet arrays

Lynna Chen,[1,a)] Jae Jung Kim,[2,a)] and Patrick S. Doyle[2,b)]
[1]*Department of Biological Engineering, Massachusetts Institute of Technology, Cambridge, Massachusetts 02139, USA*
[2]*Department of Chemical Engineering, Massachusetts Institute of Technology, Cambridge, Massachusetts 02139, USA*

(Received 31 October 2017; accepted 16 February 2018; published online 1 March 2018)

Immobilizing microscale objects (e.g., cells, spheroids, and microparticles) in arrays for direct observation and analysis is a critical step of many biological and chemical assays; however, existing techniques are often limited in their ability to precisely capture, arrange, isolate, and recollect objects of interest. In this work, we present a microfluidic platform that selectively parks microparticles in hydrodynamic traps based on particle physical characteristics (size, stiffness, and internal structure). We present an accompanying scaling analysis for the particle parking process to enable rational design of microfluidic traps and selection of operating conditions for successful parking of desired particles with specific size and elastic modulus. Our platform also enables parking of encoded particle pairs in defined spatial arrangements and subsequent isolation of these pairs in aqueous droplets, creating distinct microenvironments with no cross-contamination. In addition, we demonstrate the ability to recollect objects of interest (i.e., one particle from each pair) after observation within the channel. This integrated device is ideal for multiplexed assays or microenvironment fabrication for controlled biological studies. *Published by AIP Publishing*. https://doi.org/10.1063/1.5011342

INTRODUCTION

Microfluidic devices are ideal systems for controlled manipulation of micron-sized objects such as droplets, microparticles, and cells. Complementary length scales and precise control of flow and environmental conditions make microfluidic platforms ideal for sorting, arrangement, monitoring, and retrieval of specific objects for various biological applications. Specific examples include cell sorting[1] and droplet sorting[2,3] to separate objects of interest, single cell trapping for culturing, imaging, and downstream analysis,[4,5] paired cell immobilization for monitoring cell-cell interactions,[6–8] and immobilization of particles[9] and microorganisms[10] for bioassays.

Recently, several groups have developed microfluidic techniques that enable encapsulation of immobilized particles and cells in isolated droplets, avoiding cross-talk between droplets, and extending device capabilities for biological and chemical assays.[10–14] For example, particle-containing droplet arrays can be used for enzymatic amplification of low target signals to improve the sensitivity of hydrogel-based microRNA assays,[13] while droplet arrays encapsulating bacterial cells can be used to perform on-chip antibiograms.[10] To further improve device functionality and increase the potential for future applications, it would be advantageous to enable selective entrapment and isolation of objects with desired characteristics, as well as isolation of pairs or groups of specific objects in a deterministic manner.

Many microfluidic devices have been designed to separate objects based on physical characteristics (e.g., size, stiffness, and shape) for biological applications including circulating tumor

[a)]L. Chen and J. J. Kim contributed equally to this work.
[b)]E-mail: pdoyle@mit.edu

cell isolation and malaria diagnostics.[1,15–18] However, beyond separating one population from a complex sample, it is often useful to arrange objects of interest in designated locations within a channel[19] or microarray[20] for further observation or analysis. In addition to enabling characteristic specific arrangement of objects, it is also desirable to specifically arrange and encapsulate pairs of objects within the same compartment, in order to create highly controlled microenvironments for chemical or biological studies.

Previous groups have shown that arraying microscale objects in pairs or clusters is useful for studying interactions between cells, particles, and droplets. For example, Dura *et al.* used an array of hydrodynamic traps in a microfluidic device to pair immune cells and monitor cell-cell interactions.[8] Similar to previously reported techniques,[6,7,21] their device puts two cells in direct contact with one another using a multistep loading procedure. Other groups have used slightly different designs to pair beads[22] and droplets[23] to study diffusion reactions across an interface. However, these devices can only be used to monitor interactions based on direct contact and cannot isolate paired objects from the external environment to prevent cross-contamination. In addition, existing devices do not enable selective retrieval of specific particles (e.g., one particle from each pair) after arrangement within the channels. Another missing element from existing platforms is the lack of analysis for the object assembly process. Without design principles for how to assemble particles within traps based on particle physical properties and device operating conditions, it is difficult to translate these platforms for different applications.

In this study, we present an integrated microfluidic device for particle arrangement and isolation which overcomes the above limitations. Our device is designed to selectively immobilize (park) desired microparticles in an array of hydrodynamic traps based on three different physical characteristics (size, modulus, and internal structure), matching the highest number of sorting characteristics achievable by existing arrangement techniques.[20] Immobilized particles can then be encapsulated with high yield in aqueous droplets, isolated by an immiscible phase. This device enables long-term visualization of objects of interest in individual isolated compartments without cross-contamination. We present a scaling analysis that provides a criterion for successful particle parking, allowing for rational selection of appropriate parameters to park objects based on their physical characteristics. To our knowledge, this is the first presentation of a platform that enables the user to control parking based on particle characteristics and allows for subsequent encapsulation of these particles in isolated droplets.

We also show how to extend the design of our microfluidic device to enable precise arrangement of two different particle types in a controlled spatial configuration and demonstrate the co-encapsulation of two particles in a single aqueous droplet. In our approach, particle parking and isolation are both deterministic processes with high yield, overcoming limitations set by Poisson statistics in stochastic particle encapsulation.[24,25] Our device ensures that only desired particles are parked in designated trap locations and that all isolated droplets do not contain more than the desired number of particles, whether it is a single particle or one pair of particles. This integrated parking and isolation device eliminates the need for separate droplet generation/encapsulation and downstream sorting/merging techniques.

Another advantage of our technique is that it allows objects to be isolated in the same compartment, without being in direct contact with one another, enabling time-lapse monitoring of interactions (e.g., communication, reactions) between paired objects, while eliminating potential confounding effects arising from direct contact, including deformation, adhesion, or merging/fusion. Furthermore, after pairs have been arranged, we can selectively retrieve one particle in each pair for collection or downstream analysis. We have the ability to encode our microparticles, making it possible to track the original position of each particle within the channel. Overall, these features make our device a highly flexible platform that can be adapted for many different biological or chemical assays.

METHODS

Microfluidic device fabrication

Microfluidic devices were fabricated by previously reported procedures.[26] Briefly, polydimethylsiloxane (PDMS) (10:1 monomer to curing agent, Sylgard 184, Dow Corning) was cured

on silicon wafers patterned with SU-8 features, and devices were bonded to PDMS-coated glass slides. Three channel designs were used in this work: (1) particle synthesis channel—straight channel with a width of 300 μm and a height of 42 μm, (2) single parking spot channel (shown in Figs. 1 and 2)—serpentine channel with single trap per row (39 traps total), and (3) double parking spot channel (shown in Figs. 3 and 4)—serpentine channel with two traps per row, connected by a bridge (39 pairs total). Both types of parking channels were 38.5 μm tall.

Particle synthesis

Hydrogel microparticles were fabricated *via* stop-flow lithography.[26,27] Prepolymer solutions were prepared by mixing 20%–30% (v/v) poly(ethylene glycol) diacrylate (PEGDA; Mn = 700, Sigma-Aldrich), 5% 2-hydroxy-2-methyl-propiophenone (photoinitiator, Sigma-Aldrich), 25% de-ionized (DI) water, and 40%–50% polyethylene glycol (PEG; Mn = 200, Sigma-Aldrich) to make up the remaining volume. The ratio of PEGDA to PEG was adjusted to achieve particles of varying stiffness—the particle moduli were measured by AFM force spectroscopy to be 0.12 kPa, 0.28 kPa, and 0.65 kPa for 20%, 25%, and 30% PEGDA, respectively. To synthesize fluorescent particles, we replaced 1% (v/v) of the PEG200 with 1 mg ml^{-1} rhodamine acrylate (Polysciences) in PEG200. Using the previously reported stop flow lithography (SFL) setup,[26,27] prepolymer solution was loaded into the synthesis device by pressure-controlled flow. After stopping the flow, particles were polymerized by ultraviolet light (Thorlabs, 365 nm LED, 720 mW cm^{-2}) in mask-defined shapes (transparency masks designed in AutoCAD, printed by Fineline Imaging). The three steps (flow, stop, and exposure) were repeated to achieve semi-continuous particle synthesis. We synthesized particles carefully at low throughput to minimize variations in particle characteristics. We used circular masks to polymerize disk-shaped microparticles with diameters from 94 to 110 μm and an average height of 37 μm. We controlled the internal structure of the particles by changing the shape of the photomask to polymerize cylindrical rings with a constant outer diameter and varying internal diameters. Polymerized particles were collected from the channel outlet and purified with PBST (phosphate buffered saline with 0.05% Tween-20) by centrifugation.

MEASURING PARTICLE ELASTIC MODULUS BY ATOMIC FORCE MICROSCOPY

To determine the elastic modulus of the hydrogel microparticles, force spectroscopy measurements were performed using a MFP-3D-BIO atomic force microscope with an integrated optical microscope (Asylum Research). A 50 μl drop of particle solution (~10 particles in PBST) was placed on a glass slide. A silicon nitride cantilever of nominal spring constant 0.03 N m^{-1} with a silica spherical indenter of 600 nm diameter (Novascan) was used to indent the particles in PBST, after they settled to the surface of the slide. The inverse optical lever sensitivity (InvOLS) was calibrated from deflection-displacement curves on a rigid glass slide (41.32 nm V^{-1}), and the actual spring constant of the cantilever was measured using the thermal noise method to be 0.034 N m^{-1}.[28] For each sample, we indented 4 particles, 3 indents per particle. Elastic modulus was calculated by fitting the force-indentation curves to a maximum indentation depth of 200 nm, using the Hertz model for spherical elastic contact with IGOR data processing software (Wavemetrics). The indentation velocity was 1 μm s^{-1}. The PEGDA hydrogels were assumed to be incompressible elastic materials, with a Poisson's ratio of 0.5.[29,30] See details in the supplementary material.

CRITICAL PRESSURE MEASUREMENTS AND PARTICLE SORTING

Particle solution (concentration of ~5 particles μl^{-1} in PBST) was loaded into the inlet of the single parking spot channels using a modified pipette tip connected to a compressed air pressure source *via* Tygon tubing. Applied pressure across the device ($\Delta P_{channel}$) was precisely controlled by a Type 100LR pressure regulator and a software-controlled 3-way solenoid valve (type 6014, Burkert).[27] The pressure at the outlet of the device was atmospheric pressure. Starting from a low initial ΔP, we slowly increased ΔP until the particles of interest began to

successfully squeeze and park into the traps. If any particles were not parked, we would continue to increase ΔP by small increments until all particles in the channel were parked. For critical pressure range measurements, we used solutions containing a single particle type and recorded the pressure range required to park all particles in the channel (except for rare cases where particle parking was obstructed by debris or channel defects). We repeated this process for all particle-channel combinations (various particle diameters, moduli, and channel dimensions). For particle sorting, we used a solution containing a mixture of two particle types. Parking channels could be reused by back-flowing PBST, followed by DI water, from the outlet to the inlet at high enough pressure to remove all parked particles. Channels were then placed upside down in a shallow dish of water to ensure removal of all particles from the inlet and outlet of the device. Before reuse, channels were dried with air and baked to remove residual moisture if required. Unless otherwise specified, we report ΔP (pressure applied to the particles) for single parking spot channels and ΔP_{unit} (pressure applied to each row) for double parking spot channels (see details in the supplementary material).

ARRANGEMENT, ISOLATION, AND RECOLLECTION

For particle arrangement in double parking spot channels, we first flowed a solution containing the particle type to be parked in the inner traps. After filling all inner traps, we back-flowed PBST at low pressure to remove all excess particles, while ensuring parked particles remaining in their traps. Next, we introduced the second particle type into the channel inlet and adjusted $\Delta P_{channel}$ to park the particles in the outer traps. Particle pairs could then be isolated by back-flowing an immiscible phase (e.g., air, oil) to encapsulate particles in isolated aqueous droplets. Particles within each pair are connected via a bridge and therefore isolated within the same droplet. To selectively recollect particles, we first filled the channel with an aqueous phase to reconnect the isolated droplets. Then, we back-flowed PBST from the outlet, increasing the pressure until the desired particles were selectively recollected at the inlet, while the other particles remained in the traps.

RESULTS AND DISCUSSION

Particle parking: Design and criterion

Hydrodynamic traps in microfluidic channels have been used to array single particles, cells, embryos, and organisms for various biological applications.[31–34] The general principle relies on controlling relative fluid flow between a trap and a bypass channel.[31] When a trap is empty, a large portion of flow is directed through the trap, carrying a particle into the trap. However, once a particle occupies the trap, the resistance through the trap increases significantly. This causes the majority of flow to be redirected to the bypass channel, which carries subsequent particles to the next empty trap and ensures that each trap only contains a single particle. This is a simple and efficient method for arraying single objects in a microfluidic channel for observation and analysis. We expand on this technique by designing a modified platform that enables selective parking of particles based on physical characteristics (size, elastic modulus, and internal structure). We also develop a scaling theory to define the criterion for particle parking based on particle and trap dimensions, particle elastic modulus, and applied pressure.

To synthesize microparticles with different physical properties, we used stop flow lithography (SFL), a high-throughput method for synthesis of polymeric particles by photolithography in a microfluidic channel.[26,27] In SFL, we can precisely control the particle size and shape by changing the photomask used for UV-crosslinking and we can control the particle elastic modulus by changing the amount of crosslinker (polyethylene glycol diacrylate, PEGDA) in the prepolymer solution.[35]

To enable selective parking of microparticles based on particle physical characteristics, we designed a microfluidic device with an array of hydrodynamic traps, based on design principles from prior work.[13,31] Figure 1(a) shows the overall device design: the inlet contains a dust filter to prevent debris from entering the main channel and posts along the channel direct particles to

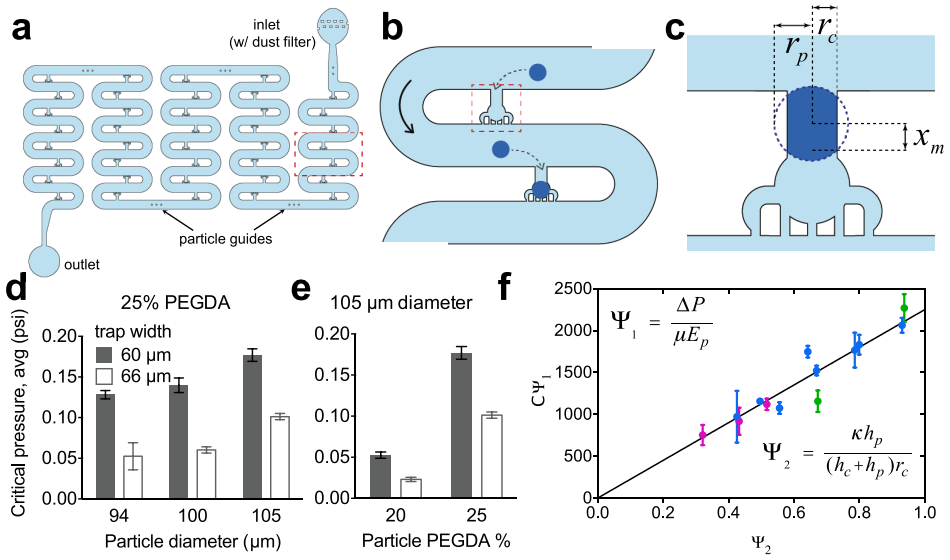

FIG. 1. Microfluidic device for microparticle arrangement. (a) Overall channel design for arrangement of particles. The device comprises an inlet and outlet with one trap per row. (b) Particles are guided by hydrodynamic force, squeezed, and parked into each trap. (c) A schematic for particle parking. (d) Plot shows the pressure required to park particles (i.e., critical pressure) of different diameters in traps with different entrance widths (all particles have the same modulus). (e) Plot shows the critical pressure to park particles with different moduli in traps with different entrance widths (all particles have the same diameter). (f) Phase diagram showing the criterion for particle parking. Different colored points represent particles of different moduli (green: 0.12 kPa, blue: 0.28 kPa, and pink: 0.65 kPa). Error bars represent the pressure range required to park all particles in the channel.

streamlines at the edge of the channel to facilitate parking into traps. There are a total of 39 traps, with one trap in each row of the serpentine channel. Figures 1(b) and 1(c) show close-up views of the hydrodynamic trap design within our device. We allocate a single trap per row, ensuring that all traps experience the same applied pressure. We control the applied pressure

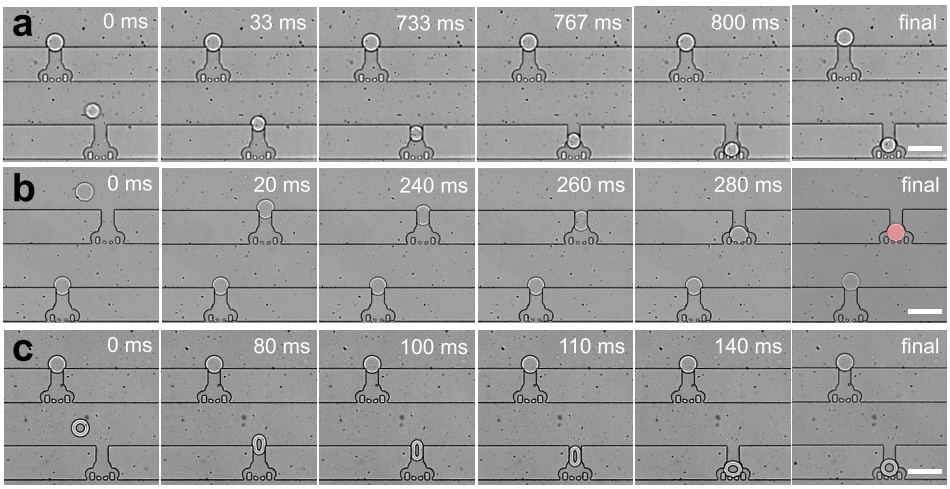

FIG. 2. Particle sorting by different physical characteristics: size (a), modulus (b), and internal structure (c). Particles with desired physical characteristics can be selectively parked into traps at a given applied pressure. (a) Small particles (89 μm, bottom trap) are successfully parked, while large particles (105 μm) are excluded at $\Delta P = 0.038$ psi. Both particles have elastic moduli of 0.28 kPa. (b) Soft particles (0.12 kPa, top trap, fluorescent) are successfully parked, while stiff particles (0.28 kPa) are excluded at $\Delta P = 0.059$ psi. The fluorescence image is overlaid in the final frame to distinguish the soft particle. Both particles are 105 μm in diameter. (c) Ring particles (29 μm thick ring with hollow interior) are successfully parked, while solid particles are excluded at $\Delta P = 0.067$ psi. Both particles have elastic moduli of 0.28 kPa and an outer diameter of 105 μm. Scale bars represent 200 μm.

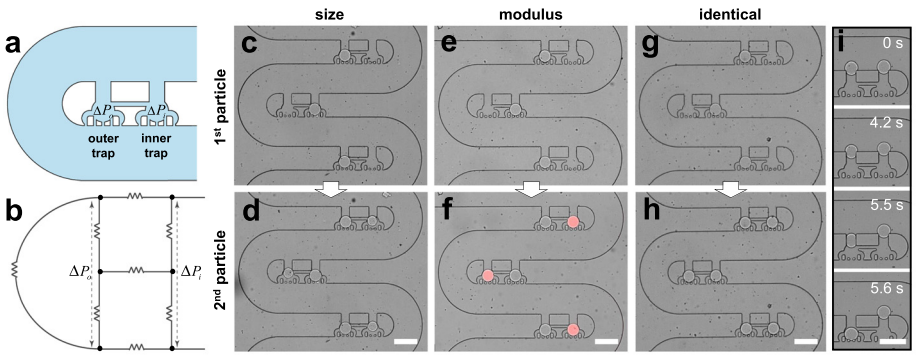

FIG. 3. Specific and sequential arrangement of particles in connected traps. (a) and (b) Schematic (a) and hydrodynamic circuit (b) of the device with one trap pair per row. Trap pair is connected by a bridge. Applied pressure along the inner trap (ΔP_i) is higher than that along the outer trap (ΔP_o), allowing sequential particle arrangement. (c) and (d) Large particles (105 μm) are first parked at the inner trap position (ΔP_{unit} =0.090 psi), and then, smaller particles (89 μm) are parked at the outer trap (ΔP_{unit} = 0.077 psi). (e) and (f) Stiff particles (0.28 kPa) are first parked at the inner trap position (ΔP_{unit} = 0.090 psi), and then, soft particles (0.12 kPa, fluorescent) are parked at the outer trap (ΔP_{unit} = 0.051 psi). (g) and (h) Identical particles are parked sequentially, first at the inner trap position (ΔP_{unit} = 0.090 psi) and then at the outer trap (ΔP_{unit} = 0.19 psi). (i) Time-lapse images showing selective parking at the inner trap position at ΔP_{unit} = 0.090 psi. Scale bars represent 200 μm.

across the entire channel ($\Delta P_{channel}$) to change the applied pressure responsible for particle parking (ΔP; details are shown in the supplementary material). Each trap contains an entrance region, the width of which can be tuned to accommodate various particles. For parking deformable hydrogel particles, we designed the entrance width (60 or 66 μm) to be smaller than the particle diameters (94–110 μm), so that particles will deform to enter the trap and remain fixed

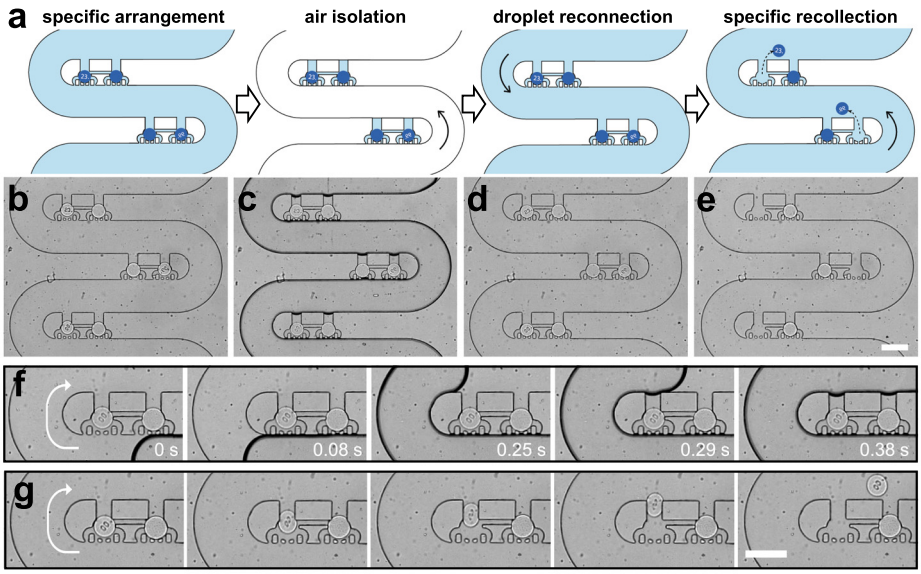

FIG. 4. Isolation and specific recollection of arranged particles. (a) Schematics of isolation and recollection processes. Traps/trap pairs can be isolated by air (or oil) to encapsulate particles within aqueous droplets in a deterministic manner. Trap pairs are connected by a bridge to allow particle pairs to reside in the same isolated droplet. Particles can also be specifically collected based on trap position or physical characteristics. (b) Arranged particles with coded particles in the outer trap position. (c) Particle pairs are isolated in aqueous droplets by back-flow of air. (d) Droplets are reconnected by forward-flow of PBST. (e) Coded particles are specifically recollected by back-flow of PBST, leaving only plain particles remaining. The original location of recollected particles can be identified by the numeric code. (f) Time-lapse images showing the isolation process by back-flow of air. Each particle pair (one coded, one plain) is isolated within the same droplet (bridge connects inner and outer trap). (g) Time-lapse images showing specific recollection of coded particles. Arrows indicate the flow direction. Scale bars represent 200 μm.

in position after parking. There are 5 pores along the bottom of each trap, each ~10 μm in width. The narrow width of each pore ensures that highly deformable particles do not pass through the bottom of the trap and prevents trespassing of the two-phase interface during the isolation process,[13] while multiple pores ensure sufficient fluid flow through the trap to guide and park particles. Figures 1(d) and 1(e) show that different critical pressures are required to park particles depending on particle diameter, trap entrance width, and particle composition. As expected, the critical pressure for parking increases with the increasing particle diameter, increasing particle modulus, or decreasing trap width. To increase the utility of our platform, we developed a scaling theory to describe all relevant parameters governing particle parking.

Based on theory developed for interference fit[36] and capillary micromechanics,[37,38] we define a dimensionless number, Ψ, that governs particle parking into the hydrodynamic trap (see derivation in the supplementary material)

$$\Psi \sim \frac{f}{F} \sim \frac{\Delta P}{\mu E_p} \frac{(h_c + h_p) r_c}{h_p \kappa}. \tag{1}$$

Ψ is the ratio of the driving force (f) to the wall friction (F). ΔP is the applied pressure difference across the particle, h_c and h_p are the channel height and particle height, respectively, r_c is half the width of the trap entrance, μ is the friction coefficient between the PDMS channel and the particle, E_p is the particle elastic modulus, and κ is defined based on particle diameter and channel width, as given below [x_m is defined in the schematic in Fig. 1(c)]

$$\kappa = 4\left[x_m - r_c \tan^{-1}\left(\frac{x_m}{r_c}\right)\right]. \tag{2}$$

The correction factor C is added to account for PDMS channel deformation,[39] which is dependent on overall applied pressure (see details in the supplementary material). Ψ can also be described as the ratio between two dimensionless groups: one describing the pressure difference and material properties (Ψ_1) and the other purely the geometric group (Ψ_2)

$$\Psi_C \sim C\Psi \sim \frac{C\Psi_1}{\Psi_2}, \tag{3}$$

$$\Psi_1 \sim \frac{\Delta P_p}{\mu E_p}, \tag{4}$$

$$\frac{1}{\Psi_2} \sim \frac{(h_c + h_p) r_c}{h_p \kappa}. \tag{5}$$

A particle will only successfully park into a trap when Ψ_C is larger than a critical value, such that the driving force overcomes wall friction. We validated this by testing many different combinations of particle size, particle modulus, and trap dimensions and determining the critical pressure for successful parking for each condition. Figure 1(f) shows a plot of $C\Psi_1$ versus Ψ_2 for different experimental conditions. We can see that all experimental data fall along a straight line, corresponding to the critical value of Ψ_C.

Selective particle parking

As particles with different physical characteristics exhibit different critical pressures for parking, we can use this device to selectively park particles with desired properties from a mixed solution. Figure 2 contains time-lapse images showing selective parking of particles with desired size, modulus, and internal structure in traps. Figure 2(a) shows parking of small particles and exclusion of larger particles at $\Delta P = 0.038$ psi. Figure 2(b) shows parking of soft particles and exclusion of stiffer particles at $\Delta P = 0.059$ psi. It is also possible to distinguish between particles of different internal structures (e.g., capsules versus solid particles), since the

internal structure contributes to overall particle deformability.[40] Figure 2(c) shows parking of ring particles with a hollow interior and exclusion of solid particles at $\Delta P = 0.067$ psi. Figure S5 (supplementary material) shows selective parking of thinner ring particles and exclusion of thicker rings. Low magnification images of channels after selective parking for each scenario are shown in Figs. S5 and S6 (supplementary material).

After parking desired particles in traps, excluded particles can be removed from the device by back-flow of PBST (from the outlet to the inlet). In this way, only selected objects will be positioned within the device for further observation or subsequent isolation in droplets. Here, we demonstrate selective parking of one particle type from a mixture of two different particles; however, it will also be possible to isolate a single particle type from a more complex mixture, as long as the desired particle requires a different critical pressure for parking compared to the other objects. Our examples show parking of the particle requiring lower critical pressure and exclusion of particles requiring higher critical pressure for parking. However, achieving the opposite case may also be possible with some design modifications. For example, if traps are designed with larger pores, soft/small particles can escape, while larger/stiffer particles remain within the traps. It should also be possible to selectively park medium size/stiffness particles by tuning relative trap entrance and pore dimensions.

The parking process is analyzed using scaling theory. Thus, the technique can be easily adapted to park other soft biological objects (e.g., cells, spheroids, and embryos), by scaling the device to the relevant dimensions. For smaller objects, it might be required to use other fabrication techniques, such as etching or e-beam lithography, to scale down the device. A scaling analysis may require slight modifications to account for differences in the object shape/structure. Since physical properties can often be used to identify cell type or cell state, the ability to selectively park and monitor cells with specific physical characteristics may be extremely useful for fundamental biological studies or diagnostics applications.

Sequential particle arrangement

By increasing the number of traps per row, we can enable proximal particle arrangement in a specific and sequential manner. We can take advantage of the fact that the trap position along each row of the channel influences the $\Delta P_{channel}$ required for particle parking. As shown in Figs. 3(a) and 3(b), the applied pressure along the inner trap position (ΔP_i) is higher than the outer trap (ΔP_o) at a given ΔP_{unit} (=applied pressure over each row). This means that for the same particle, a lower ΔP_{unit} is required to park the particle at the inner trap position compared to the outer trap. This enables us to sequentially park identical particles or arrange two different particles at specific locations.

Figures 3(c) and 3(d) show initial parking of large particles at the inner trap position, followed by parking of small particles at the outer trap. Between these two steps, excess large particles are removed from the channel by back-flowing PBST at a low pressure. Similarly, in Figs. 3(e) and 3(f), stiff particles are first parked at the inner trap, followed by soft particles at the outer trap. Note that the positions of the two particle types can be easily swapped by changing the parking sequence (e.g., first park soft particles at the inner trap, followed by stiff particles at the outer trap). These examples demonstrate specific arrangement of particles with different physical characteristics, but the device can also be used to arrange identical particles in a sequential manner, as shown in Figs. 3(g) and 3(h). First, all inner traps are filled at a low ΔP_{unit} [0.090 psi; time-lapse images shown in Fig. 3(i)], and then, ΔP_{unit} is increased (0.19 psi) to park particles at the outer trap location. This would potentially be useful for arraying particles with the same physical properties but different chemical/biological functionalities.

The two traps in each row can be connected via a bridge (as shown in Fig. 3), so that upon isolation the paired objects will reside in the same droplet, and it will be possible to monitor interactions between the two objects. Compared to previous microfluidic platforms[6,11,21] for arranging pairs or groups of objects, the two particles in our device do not have to come into direct contact with one another. This means that it is possible to monitor longer-range interactions between objects that may be distinct from interactions arising from direct contact. For

example, our device could be used for distinguishing cell-cell communication through secreted signaling molecules, rather than membrane contact,[41] on a single cell level. Inter-trap/inter-particle distance can also be tuned for various applications. It should be noted that larger distances between traps would result in a greater difference in required ΔP_{unit} to park particles in each of the two trap sites. This platform can also be easily extended for arrangement of more than two particles by addition of more trap sites along each row of the channel. This is an inherent limitation of many other platforms due to particle loading design.

Particle isolation and recollection

Our platform enables parking and isolation of particles within aqueous droplets in a deterministic manner, with high yield for both processes, as shown in our group's recent demonstration of a device with similar design principles.[13] Efficient isolation of particles (>95% of parked particles are isolated) was performed by back-flowing immiscible oil from the device outlet to inlet, encapsulating particles in water-in-oil droplets in the process. Back-flow was used to prevent the oil-water interface from trespassing the trap, ensuring homogeneous droplet sizes, and preventing deformation of soft particles. This is because the pressure due to interfacial tension between oil and water is much higher at the narrow trap pores ($\sim$10 μm in width) compared to the wider trap entrance ($\sim$60 μm). The trap entrance and pore dimensions are designed to enable particles to park within the trap without escaping. As demonstrated by a scaling theory,[13] allowing the oil to pass by the trap pores before the entrance prevents trespassing of the interface (maximum interfacial tension > applied pressure) and ensures uniform-sized droplets, independent of particle stiffness.

In the platform presented here, we demonstrate efficient isolation using air to create water-in-air droplets. After isolation, droplets can be reconnected, and particles can be specifically recollected. Figure 4(a) shows a schematic of the overall process and the flow direction for each step of the process. Figures 4(b)–4(e) show the corresponding experimental images: Fig. 4(b) shows the device after specific arrangement of two particle types—particles with a numeric code are parked in the outer trap, while plain particles are parked in the inner trap; Fig. 4(c) shows the particle pairs after isolation in droplets by back-flow of air; Fig. 4(d) shows the channel after droplets have been reconnected by forward-flow of PBST; Fig. 4(e) shows the channel after specific recollection of coded particles from the outer trap location.

Figure 4(f) and Video S1 (supplementary material) show the isolation process in detail. The air-water interface can be seen flowing from the bottom of the traps around to the top, encapsulating particle pairs in aqueous droplets in the process. It is clear that the interface does not penetrate the traps and that particles remain fixed in their positions (the applied pressure for isolation should be lower than the pressure for particle escaping from both traps). After isolation, the particle pairs show no deformation and clearly reside in the same isolated droplet via the connecting bridge. We can easily replace air with an immiscible oil to create water-in-oil droplets instead.[13]

Figure 4(g) and Video S2 (supplementary material) show the particle recollection process. By back-flowing PBST at an applied pressure greater than the escaping pressure for the outer trap but lower than the escaping pressure for the inner trap, only coded particles in the outer trap can be selectively collected at the inlet. By increasing the pressure, both particle types can be collected together or sequentially—plain particles after coded particles. The ability to encode SFL particles[42] allows us to track the original particle location within the channel. This is beneficial for generating distinct, parallelized microenvironments, where we are able to analyze objects after recollection.

The ability to park and isolate pairs or groups of objects in specific proximal arrangements is ideal for microenvironment fabrication. For example, drug or chemical containing particles can be parked in one trap, while cell-coated[43] or cell-containing[44] particles can be parked in the neighboring trap. Or, a scaled-down device may be used to monitor interactions between single cells of different cell types. Isolation enables long-term monitoring of object pairs without crosstalk between pairs in the same channel. This also enables multiplexed assays or

accumulation of reaction products within individual droplets. The ability to easily recollect one specific object from each pair after arrangement within the channel is an additional advantage of this platform—this could enable separate downstream analysis of the two particle types after a reaction in the isolated droplet.

CONCLUSION

We demonstrate a microfluidic device for characteristic-specific parking of soft microparticles and sequential arrangement of microparticle pairs to create isolated microenvironments. We present a scaling analysis for the parking process of deformable microparticles into the hydrodynamic traps, enabling rational selection of operating conditions for the arrangement of particles with different sizes and stiffness. After desired particles are parked in the trap array, single or paired particles can be easily isolated in aqueous droplets by back-flowing an immiscible phase through the channel. Based on our design, particles are encapsulated in monodisperse droplets with high yield, enabling multiplexed assays within the channel with no crosstalk. Our design could also be extended to park and isolate groups of three or more particles, with tunable inter-particle spacing. Our simple and inexpensive PDMS-based channel design, with one inlet and one outlet, is easy to operate and ensures robust fabrication of particle-in-droplet arrays without the need for multiple devices for droplet generation, droplet sorting, and droplet arrangement. The trap design can be easily tailored for specific applications—for example, scaling down dimensions to create arrays of uniform-sized deformable cells,[4,12] excluding cells above a certain size or stiffness. We also demonstrate the ability to specifically recollect encoded particles from our arrays, based on their parking position. The use of encoded particles synthesized by SFL enables tracking of particle position throughout any multistep assays. This flexible platform can be easily extended for future applications requiring arrangement and isolation of soft, biological objects.

SUPPLEMENTARY MATERIAL

See supplementary material for detailed information of methods, derivation of scaling analysis, and additional experimental data.

ACKNOWLEDGMENTS

We gratefully acknowledge funding from NIH Grant 1R21EB024101-01, a Samsung Scholarship to J.J.K., and an NSERC fellowship to L.C. Microfabrication was performed at MIT's Microsystems Technology Laboratories, and AFM experiments were conducted in the NanoLab, MIT. We thank A. Schwartzman and B. Qing for insightful discussions.

[1]J. P. Beech, S. H. Holm, K. Adolfsson, and J. O. Tegenfeldt, Lab Chip **12**, 1048 (2012).
[2]M. Chabert and J. Viovy, Proc. Natl. Acad. Sci. U.S.A. **105**, 3191 (2008).
[3]S.-Y. Teh, R. Lin, L.-H. Hung, and A. P. Lee, Lab Chip **8**, 198 (2008).
[4]K. Chung, C. A. Rivet, M. L. Kemp, and H. Lu, Anal. Chem. **83**, 7044 (2011).
[5]R. J. Kimmerling, G. Lee Szeto, J. W. Li, A. S. Genshaft, S. W. Kazer, K. R. Payer, J. de Riba Borrajo, P. C. Blainey, D. J. Irvine, A. K. Shalek, and S. R. Manalis, Nat. Commun. **7**, 10220 (2016).
[6]P. J. Lee, P. J. Hung, R. Shaw, L. Jan, and L. P. Lee, Appl. Phys. Lett. **86**, 223902 (2005).
[7]J.-P. Frimat, M. Becker, Y.-Y. Chiang, U. Marggraf, D. Janasek, J. G. Hengstler, J. Franzke, and J. West, Lab Chip **11**, 231 (2011).
[8]B. Dura, S. K. Dougan, M. Barisa, M. M. Hoehl, C. T. Lo, H. L. Ploegh, and J. Voldman, Nat. Commun. **6**, 5940 (2015).
[9]S. Y. Yeom, C. H. Son, B. S. Kim, S. H. Tag, E. Nam, H. Shin, S. H. Kim, H. Gang, H. J. Lee, J. Choi, H.-I. Im, I.-J. Cho, and N. Choi, Anal. Chem. **88**, 4259 (2016).
[10]G. Amselem, C. Guermonprez, B. Drogue, S. Michelin, and C. N. Baroud, Lab Chip **16**, 4200 (2016).
[11]H. Kim, S. Lee, W. Lee, and J. Kim, Adv. Mater. **29**, 1701351 (2017).
[12]M. Sauzade and E. Brouzes, Lab Chip **17**, 2186 (2017).
[13]J. J. Kim, L. Chen, and P. S. Doyle, Lab Chip **17**, 3120 (2017).
[14]S. Sart, R. F. Tomasi, G. Amselem, and C. N. Baroud, Nat. Commun. **8**, 469 (2017).
[15]Z. T. F. Yu, K. M. Aw Yong, and J. Fu, Small **10**, 1687 (2014).
[16]B. D. Plouffe and S. K. Murthy, Anal. Chem. **86**, 11481 (2014).
[17]E. Ozkumur, A. M. Shah, J. C. Ciciliano, B. L. Emmink, D. T. Miyamoto, E. Brachtel, M. Yu, P. Chen, B. Morgan, J. Trautwein, A. Kimura, S. Sengupta, S. L. Stott, N. M. Karabacak, T. A. Barber, J. R. Walsh, K. Smith, P. S. Spuhler, J. P.

Sullivan, R. J. Lee, D. T. Ting, X. Luo, A. T. Shaw, A. Bardia, L. V. Sequist, D. N. Louis, S. Maheswaran, R. Kapur, D. A. Haber, and M. Toner, Sci. Transl. Med. **5**, 179ra47 (2013).
[18]H. W. Hou, A. A. S. Bhagat, A. G. L. Chong, P. Mao, K. S. W. Tan, J. Han, and C. T. Lim, Lab Chip **10**, 2605 (2010).
[19]J. Kim, J. Erath, A. Rodriguez, and C. Yang, Lab Chip **14**, 2480 (2014).
[20]J. J. Kim, K. W. Bong, E. Reátegui, D. Irimia, and P. S. Doyle, Nat. Mater. **16**, 139 (2017).
[21]A. M. Skelley, O. Kirak, H. Suh, R. Jaenisch, and J. Voldman, Nat. Methods **6**, 147 (2009).
[22]T. Teshima, H. Ishihara, K. Iwai, A. Adachi, and S. Takeuchi, Lab Chip **10**, 2443 (2010).
[23]Y. Bai, X. He, D. Liu, S. N. Patil, D. Bratton, A. Huebner, F. Hollfelder, and W. T. S. Huck, Lab Chip **10**, 1281 (2010).
[24]D. J. Collins, A. Neild, A. Liu, and Y. Ai, Lab Chip **15**, 3439 (2015).
[25]T. P. Lagus and J. F. Edd, RSC Adv. **3**, 20512 (2013).
[26]D. Dendukuri, D. C. Pregibon, J. Collins, T. A. Hatton, and P. S. Doyle, Nat. Mater. **5**, 365 (2006).
[27]D. Dendukuri, S. S. Gu, D. C. Pregibon, T. A. Hatton, and P. S. Doyle, Lab Chip **7**, 818 (2007).
[28]J. L. Hutter, J. Bechhoefer, J. L. Hutter, and J. Bechhoefer, Rev. Sci. Instrum. **64**, 1868 (1993).
[29]K. S. Anseth, C. N. Bowman, and L. Brannon-Peppas, Biomaterials **17**, 1647 (1996).
[30]D. L. Elbert and J. A. Hubbell, Biomacromolecules **2**, 430 (2001).
[31]W.-H. Tan and S. Takeuchi, Proc. Natl. Acad. Sci. U.S.A. **104**, 1146 (2007).
[32]S. Kobel, A. Valero, J. Latt, P. Renaud, and M. Lutolf, Lab Chip **10**, 857 (2010).
[33]W. Shi, J. Qin, N. Ye, and B. Lin, Lab Chip **8**, 1432 (2008).
[34]K. Chung, Y. Kim, J. S. Kanodia, E. Gong, S. Y. Shvartsman, and H. Lu, Nature Methods **8**, 171 (2011).
[35]R. Haghgooie, M. Toner, and P. S. Doyle, Macromol. Rapid Commun. **31**, 128 (2010).
[36]B. Hamrock, B. Jacobson, and S. Schmid, *Fundamentals of Machine Elements* (McGraw-Hill, 1999).
[37]H. M. Wyss, T. Franke, E. Mele, and D. A. Weitz, Soft Matter **6**, 4550 (2010).
[38]M. Guo and H. M. Wyss, Macromol. Mater. Eng. **296**, 223 (2011).
[39]T. Gervais, J. El-Ali, A. Günther, and K. F. Jensen, Lab Chip **6**, 500 (2006).
[40]L. Chen, K. X. Wang, and P. S. Doyle, Soft Matter **13**, 1920 (2017).
[41]E. E. Hui and S. N. Bhatia, Proc. Natl. Acad. Sci. U.S.A. **104**, 5722 (2007).
[42]D. C. Pregibon, M. Toner, and P. S. Doyle, Science **315**, 1393 (2007).
[43]K. W. Bong, J. J. Kim, H. Cho, E. Lim, P. S. Doyle, and D. Irimia, Langmuir **31**, 13165 (2015).
[44]P. Panda, A. Shamsher, E. Lo, B. G. Chung, T. A. Hatton, A. Khademhosseini, and P. S. Doyle, Lab Chip **8**, 1056 (2008).